Electrochimica Acta 68 (2012) 44–51

Contents lists available at SciVerse ScienceDirect

Electrochimica Acta

journal homepage: www.elsevier.com/locate/electacta

Characterization of 2,(3)-tetra-(4-oxo-benzamide) phthalocyaninato cobalt (II)–Single walled carbon nanotube conjugate platforms and their use in electrocatalysis of amitrole

Tawanda Mugadza, Yasin Arslanoğlu, Tebello Nyokong*

Department of Chemistry, Rhodes University, P.O. Box 94, Grahamstown 6140, South Africa

ARTICLE INFO

Article history:
Received 2 November 2011
Received in revised form 11 January 2012
Accepted 6 February 2012
Available online 19 February 2012

Keywords:
Single walled carbon nanotubes
Cobalt (II) phthalocyanine
Amitrole
Voltammetry
Chronoamperometry

ABSTRACT

In this paper we report on the use of carboxylic acid functionalized single walled carbon nanotubes (SWCNT) in the synthesis of 2,(3)-tetra-(4-oxo-benzamide)phthalocyaninato cobalt (II)–single walled carbon nanotube conjugates (CoTOBPc–SWCNT), their characterization and application in the electrocatalytic oxidation of amitrole. Cyclic voltammetry, chronoamperometry and electrochemical impedance spectroscopy were used for the detection of amitrole on the modified glassy carbon electrode. The catalytic rate constant was $1.6 \times 10^3\ M^{-1}\ s^{-1}$ and the apparent electron rate transfer constant was $1.5 \times 10^{-5}\ cm\ s^{-1}$. The linear dynamic range was 1.0×10^{-6}–3.0×10^{-5} M, with a sensitivity of $\sim 1.13\ A\ mol^{-1}\ L\ cm^{-2}$.

1. Introduction

The unique behaviour of carbon nanotubes (CNTs) include their remarkable electrical, chemical, mechanical and structural properties that make them a very attractive material for a wide range of applications [1–3] including the successful enzymatic detection of pesticides and nerve agents [4]. Single walled carbon nanotubes (SWCNTs) offer advantages such as high surface area, good conductance, favourable electronic properties and electrocatalytic effects making them suitable for use as electrochemical sensors and biosensors [5].

Metallophthalocyanines (MPcs) are used in the fabrication of electrochemical sensors due to their exceptional physicochemical, electronic and electro-catalytic properties. The combination of CNTs and Pcs carrying electroactive metal centres is opening up a lot possibilities for their application as mediators in electrocatalysis. SWCNTs have been modified with MPcs through electropolymerization [6], electrosorption [7], chemical conjugation [8,9] and simply by adsorption [10]. The Pc-SWCNT composites have been used as sensors for the detection of nitrite [11], nerve agents [12], pesticides [8], 2-mercaptoethanol [9], hydrazine [10] and for oxygen and hydrogen peroxide reduction [13,14]. Electrodes modified with SWCNTs mixed with MPcs are known to be stable for analyses [15]. Both MPcs and SWCNTs have been observed to have synergistic effect on each other in terms of reactivity towards analytes [8,10,12], as evidenced by reduction in oxidation overpotentials and improved catalytic currents.

In this work we report on the synthesis of (2,(3)-tetra-(4-oxo-benzamide)phthalocyaninato cobalt (II) (CoTOBPc, Scheme 1) and its chemical linking to SWCNTs to give CoTOBPc–SWCNT, Scheme 2. The latter is employed for the electrocatalysis of amitrole (3-amino-1,2,4-triazole).

SWCNTs have been linked to the more readily available tetraamino phthalocyanines, which have low solubility or to unsymmetrically substituted phthalocyanines containing one amino functionality [8,9,16]. The latter are very challenging to synthesize in addition to problems with solubility. Hence, in this work we report on a new complex CoTOBPc, which is tetrasubstituted with 4-oxobenzamide groups which increases the solubility of the Pc and encourage formation of chemical linkages with carboxylic acid functionalized SWCNTs. Chemical linkages are important in increasing the dispersion of SWCNTs which are not very soluble. Also the new complex contains imide bonds between Pc and the SWCNT which have never been reported before.

The imide linkages formed between CoTOBPc and SWCNT serve as a bridge for the smooth transfer of electrons to and from the SWCNTs, hence the observed improvements in electrocatalytic performances. Amitrole is a toxic non-selective herbicide used to control weeds in agriculture [17]. Multi-walled carbon nanotubes paste electrodes [18], combined multi-walled

* Corresponding author. Tel.: +27 46 6038260; fax: +27 46 6225109.
E-mail address: t.nyokong@ru.ac.za (T. Nyokong).

0013-4686/$ – see front matter © 2012 Elsevier Ltd. All rights reserved.
doi:10.1016/j.electacta.2012.02.041

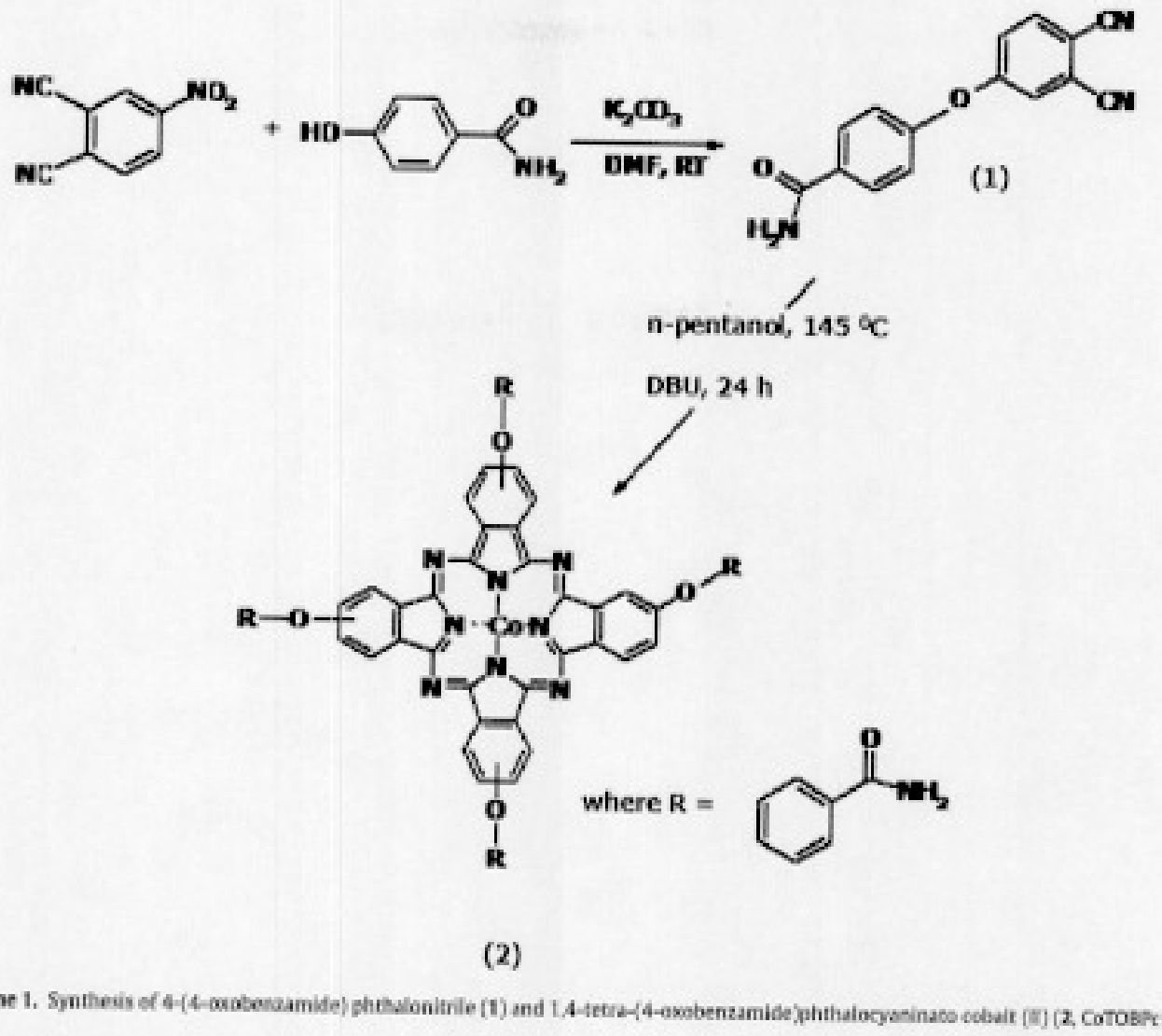

(2)

Scheme 1. Synthesis of 4-(4-oxobenzamide) phthalonitrile (1) and 1,4-tetra-(4-oxobenzamide)phthalocyaninato cobalt (II) (2, CoTOBPc).

carbon nanotube-iron tetraamino-phthalocyanine electrodes [19] and nafion/lead-ruthenium oxide pyrochlore chemically modified electrodes [20] have been used in the electrochemical detection of amitrole. This work aims at using amitrole as a test molecule for the effectiveness of the CoTOBPc–SWCNT conjugate in lowering potentials.

2. Experimental

2.1. Chemicals and reagents

Single walled carbon nanotubes (SWCNTs, 2–10 nm in diameter and 1–5 μm in length, purity (40–60% carbon content), potassium carbonate, 1,8-diazabicyclo[5.4.0]undec-7-ene (DBU), amitrole, tetrabutyl ammonium tetrafluoroborate ($TBABF_4$), 4-oxobenzamide and pH 4 buffer tablets were obtained from Aldrich. $SOCl_2$ was obtained from Merck. 4-Nitrophthalonitrile was prepared according to literature [21]. Dimethylformamide (DMF) and tetrahydrofuran (THF) were from Merck and were freshly dried and distilled before use. Aqueous solutions were prepared using Millipore water from Milli-Q Water Systems (Millipore Corp., Bedford, MA, USA, conductivity range = 0.055–0.294 μS/cm). All other chemicals and reagents were of analytical grade and were used as received. A stock solution of 1×10^{-3} M amitrole was prepared by dissolving the pesticide in methanol and later used to prepare standards using pH 4 buffer. All other reagents were obtained from suppliers and used as received.

2.2. Equipment

All electrochemical experiments (cyclic voltammetry, square wave voltammetry, chronoamperometry and electrochemical impedance spectroscopy) were performed using Autolab potentiostat PGSTAT 302 (Eco Chemie, Utrecht, The Netherlands) driven by the general purpose electrochemical system data processing software (GPES, version 4.9). Square wave voltammetric analysis was carried out at a frequency of 10 Hz, amplitude: 50 mV and step potential: 5 mV. A three electrode electrochemical cell comprising of glassy carbon electrode (GCE) as the working electrode (geometric area = 0.071 cm^2), platinum wire (Pt) as a counter electrode and a silver|silver chloride wire (Ag|AgCl) as a pseudo-reference electrode was used. The potential response of Ag|AgCl pseudo-reference in aqueous conditions was less than the Ag|AgCl (3 M KCl) by 0.015 ± 0.003 V. The optically transparent thin-layer electrochemical(OTTLE)cell connected to a Bioanalytical Systems (BAS) CV 27 voltammograph was used in spectroelectrochemical studies.

Shimadzu UV-2550 spectrophotometer, Perkin Elmer FTIR spectrometer and Bruker Vertex 70-Ram II spectrometer (equipped with a 1064 nm Nd:YAG laser and a liquid nitrogen cooled germanium detector) were used to collect UV–vis, infrared and Raman data respectively. X-ray diffraction (XRD) spectroscopic data were obtained using the Bruker XRD (Discovery D8 MR). The XRD, FTIR and Raman spectral data for the raw SWCNTs, functionalized SWCNTs (SWCNT-COOH), CoTOBPc, CoTOBPc–SWCNT, CoTOBPc/SWCNT were obtained in their solid forms.

2.3. Synthesis

2.3.1. Synthesis of 4-(4-oxobenzamide) phthalonitrile (1, Scheme 1)

4-Hydroxybenzamide (2.74 g, 20 mmol) and 4-nitrophthalonitrile (3.46 g, 20 mmol) were dissolved in DMF (30 mL) and the mixture stirred at room temperature for 30 min

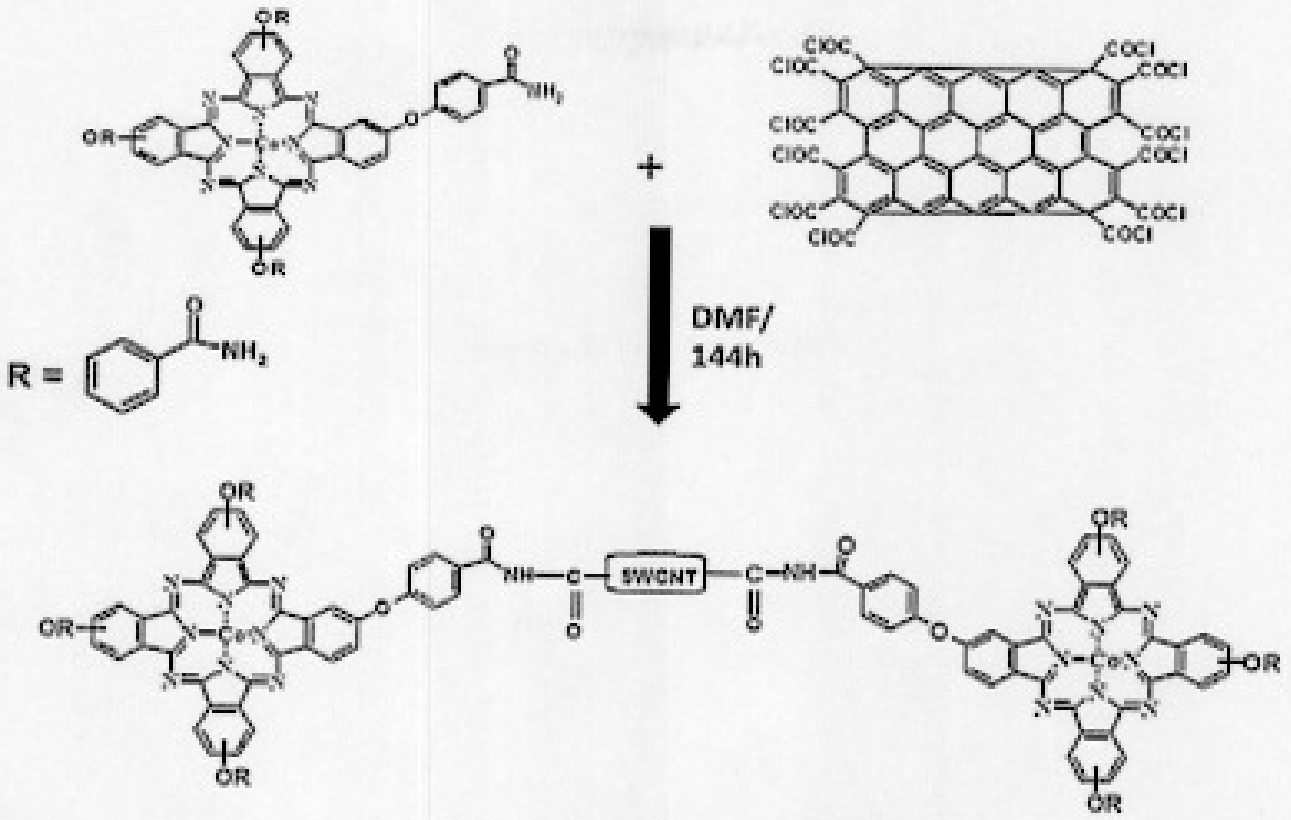

Scheme 2. Coordination of CoTOBPc to SWCNT.

under nitrogen. Thereafter, finely ground K_2CO_3 (6.85 g, 50 mmol) was added portion-wise over a period of 4 h. The reaction mixture was then stirred under nitrogen at room temperature for 36 h. The resulting mixture was added to water (100 mL) and stirred for 30 min. The resultant precipitate was filtered off, thoroughly washed with water, dried and recrystallized from ethanol. M.p.: 220 °C Yield: 3.17 g (60%). FT-IR ν_{max}/cm^{-1}: 3400 (NH_2), 3286–3065 (Ar–CH), 2236 (C≡N), 1646 (C=O), 1256 (C–O–C), 1179. ^1H NMR ($CDCl_3$): δ, ppm 8.38–8.36 (d, 1H, Ar–H), 8.24–8.22 (d, 2H, Ar–H), 8.12–8.11 (d, 1H, Ar–H), 7.73–7.71 (d, 1H, Ar–H), 7.64 (s, 2H, NH_2), 7.49–7.48 (d, 2H, Ar–H). ^{13}C NMR (DMSO): δ, ppm 167.58 (C=O), 160.98, 157.12, 137.07, 131.04, 130.79, 124.12, 123.59, 120.22, 117.52 (C≡N), 116.55, 116.04, 109.57. Calc. for $C_{15}H_9N_3O_3$: C 68.44, H 3.45, N 15.96; Found: C 68.20, H 2.80, N 16.17. MS (ESI-MS) *m/z*: Calc. 263.2; Found: 264.3 $[M+H]^+$.

2.3.2. Synthesis of 1,4-tetra-(4-oxobenzamide)phthalocyaninato cobalt (II) (2), CoTOBPc, Scheme 1

A mixture of 4-(4-oxobenzamide) phthalonitrile (**1**) (0.26 g, 1 mmol), anhydrous cobalt (II) chloride (0.07 g, 0.5 mmol), DBU (0.15 mL, 1.0 mmol) and dry n-pentanol (3 mL) was heated and stirred at 100 °C for approximately 0.5 h under nitrogen. The reaction tube was sealed and reaction continued at 145 °C for 24 h under nitrogen atmosphere. After cooling to room mixture, the solution was poured into a methanol/water (1:1) mixture to precipitate the crude product. The dark blue product was collected by filtration and washed with acetone followed with n-hexane. The pure product was isolated using column chromatography on silica gel and methanol (MeOH) as the eluent. The product was further purified on silica gel using $CHCl_3$/MeOH (1:1) as the eluting solvent.

Yield: 0.11 g, 39%. M.p. > 200 °C. FT-IR ν_{max}/cm^{-1}: 3414 (NH_2), 3185–2955 (Ar–H), 1659 (C=O), 1602 (C=C), 1227 (C–O–C), 1163, 849. UV–VIS λ_{max} (nm) (log ε) in DMF: 330 (4.37), 604 (4.19), 666 (4.93). Anal. Calcd. for $C_{60}H_{36}N_{12}O_8Co$: C, 64.81; H, 3.26; N, 15.12. Found: C, 64.75; H, 3.22; N, 15.01. MALDI-TOF MS *m/z*: Calcd: 1111.2 amu; Found: $[M+H]^+$ 1112.2 amu.

2.3.3. Synthesis of polyimide CoTOBPc–SWCNT conjugates (3, Scheme 2)

SWCNTs were carboxylic acid functionalized according to literature [22] and converted to SWCNT–COCl as reported [12,23].

The SWCNT-COCl was then refluxed with 0.1 g CoTOBPc in 15 mL of DMF for 144 h. The resulting solid was centrifuged for 20 min, DMF decanted and the solid washed thoroughly with several portions of DMF to remove excess CoTOBPc. The resultant polyimide (CoTOBPc–SWCNT) was further washed with ethanol and the solid product was dried at room temperature under vacuum.

2.4. Electrochemical methods

Before use, the glassy carbon electrode (GCE) was polished on a Buehler-felt pad using alumina (0.05 μm), and then washed with millipore water, sonicated for 5 min in millipore water, washed again with millipore water and then with pH 4 buffer solution. The GCE was modified with SWCNT-COOH, CoTOBPc, CoTOBPc–SWCNT and a mixture (without a chemical bond) of CoTOBPc and SWCNT-COOH (CoTOBPc/SWCNT), represented as SWCNT–GCE, CoTOBPc–GCE, CoTOBPc–SWCNT–GCE and CoTOBPc/SWCNT–GCE, respectively. The modifiers were dispersed in DMF through ultrasonication for 1 h. The drop and dry method was used to modify the GCE. The modified electrode was then rinsed in pH 4 buffer solution before analysis. All solutions for voltammetric studies were prepared in pH 4 buffer. Prior to the analyses all the solutions were purged with argon gas to drive out oxygen and an atmosphere of argon was maintained throughout the analyses. Before use for analyses, the modified electrodes were scanned between 0.0 V and 1.0 V (versus Ag/AgCl (3 M KCl)) in pH 4 buffer solution to obtain stable cyclic voltammograms.

3. Results and discussion

Scheme 1 shows the synthetic pathways for the phthalonitrile (**1**) and phthalocyanine (**2**) used in this work. The phthalocyanine complex **2** was formed by cyclotetramerization of compound **1**. Complex **2** was characterized by FT-IR, UV–Vis, MALDI-TOF-MS

and elemental analysis. The results obtained were in agreement with the predicted structure given in Scheme 1. Peripherally substituted complexes always occur as a mixture of isomers which are difficult to separate. Scheme 2 represents the possible structure formed between SWCNT and CoTOBPc. Because of differences in size between SWCNT and CoTOBPc, the most possible structure is the one where the former is the centre and Pcs are coordinated to it. The structure where more than one SWCNT is coordinated to the Pc is not viable because of the much smaller size of the latter.

3.1. Spectroscopic characterizations

The Q-bands for CoTOBPc/SWCNT and CoTOBPc–SWCNT are red-shifted at 667 and 670 nm respectively relative to CoTOBPc whose absorption maximum is at 659 nm, Table 1. The red-shifting of 8 nm and 11 nm for the mixture and the conjugate respectively, is a confirmation of the interaction between the CoTOBPc and the SWCNTs and has been observed before and possibly due to π–π interactions [24] for the former and chemical linking in the latter [25].

Fig. 1 (Supporting information) shows the FTIR spectra for SWCNT-COOH, CoTOBPc–SWCNT and CoTOBPc. The C=O band for CoTOBPc is observed at 1659 cm^{-1}. The shift of C=O stretch for CoTOBPc (1659 cm^{-1}) to 1618 cm^{-1} for CoTOBPc–SWCNT confirms linking between CoTOBPc and SWCNT-COOH. The C=O stretch for SWCNT-COOH is at 1639 cm^{-1}.

Fig. 2a–c (Supporting information) shows the Raman spectra for CoTOBPc, SWCNT-COOH and CoTOBPc–SWCNT, respectively. The G band was observed in the range 1545–1600 cm^{-1} as in other studies [26], while the D band was found around 1292 cm^{-1} for CoTOBPc–SWCNT and SWCNT-COOH. The D-band for the CoTOBPc was observed at 1341 cm^{-1} and is in agreement with literature [26]. There is significant increase in the D- and G-bands intensities which are also accompanied by peak shifts for the conjugate relative to the SWCNT-COOH, an indication of the incorporation of the CoTOBPc in the SWCNT structure.

Fig. 3 (Supporting information) shows the XRD spectral data for CoTOBPc, SWCNT-COOH and CoTOBPc–SWCNT. The XRD spectrum for CoTOBPc has one peak at around 27.2°, which is typical of phthalocyanines [27], while the SWCNT showed three peaks at 2θ-values of 26.0°, 42.5° and 53.5° [28]. The shift in peak on conjugation could be due to the formation of a new crystal structure. The formation of a new crystal structure is further confirmed by the presence of a new peak at 2θ = 18.0°.

3.2. Cyclic voltammetry and spectroelectrochemical characterization of CoTOBPc in solution

Fig. 1 shows the cyclic (a) and square wave voltammograms (b) for bare GCE in 1 mM CoTOBPc (DMF) in the presence of 0.1 M $TBABF_4$ as a supporting electrolyte. Three distinctly resolved redox processes (**I**, **II** and **III**) were observed, Fig. 1. Couple **I** has an $E_{1/2} = -0.42$ V, while processes **II** and **III** are at potentials +0.45 V (E_p) and +1.05 V ($E_{1/2}$), respectively, versus Ag/AgCl. Couple **I** and process **II** are metal-based redox processes, while process **III** is ring-based, in accordance with literature for CoPc complexes in DMF [29]. In this paper, only spectral changes for process **II** were undertaken in order to determine the species that were involved in the catalysis of amitrole. Upon oxidation (at potential of process **II**), there was a red-shift in Q-band position (from 664 to 667 nm, figure not shown) with no significant change in intensity. Such spectral transformations are in agreement with the oxidation of Co^{II} to Co^{III} species and this confirms the assignment of peak II to $Co^{III}Pc^{-2}/Co^{II}Pc^{-2}$ process as observed in other studies [30].

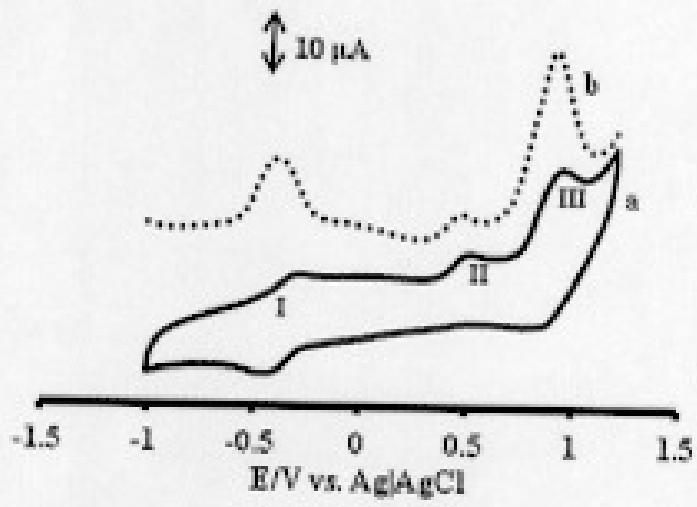

Fig. 1. (a) Cyclic voltammogram (scan rate = 100 mV/s) and (b) square wave voltammogram (frequency = 10 Hz, amplitude = 50 mV and step potential = 5 mV) for bare GCE in 1 mM CoTOBPc. Supporting electrolyte = 0.1 M $TBABF_4$.

3.3. Surface characterization

3.3.1. Electrode behaviours in $[Fe(CN)_6]^{3-/4-}$ redox probe

The comparative CVs for the modified glassy carbon electrodes used in this work in were done in the presence of the $[Fe(CN)_6]^{3-/4-}$ redox probe (figure not shown, but data in Table 1). The cathodic to anodic peak potential separation (ΔE_p) for bare GCE, CoTOBPc–SWCNT–GCE, CoTOBPc/SWCNT–GCE, SWCNT–GCE and CoTOBPc–GCE are 64 mV, 61 mV, 75 mV, 69 mV and 80 mV (versus Ag/AgCl) respectively at a scan rate of 50 mV/s, Table 1. These ΔE_p values indicate that the electrode modifiers did not inhibit the flow of electrons, and as such they could be used as reaction mediators in electrocatalysis. The order in terms of electron transfer efficiency is therefore CoTOBPc–SWCNT–GCE > bare GCE > SWCNT–GCE > CoTOBPc/SWCNT–GCE > CoTOBPc–GCE, confirming the good electron transfer kinetics for the linked complex compared to the rest of the modified electrodes, including the bare GCE. The smaller ΔE_p value for CoTOBPc–SWCNT–GCE (61 mV) is indicative of the presence of linkages between the CoTOBPc and the SWCNTs which facilitate the easy exchange of electrons between the analyte and the electrode. Using the cyclic voltammograms of $[Fe(CN)_6]^{4-/3-}$ in 0.1 M of KCl and applying the Randles–Sevcik Eq. (1) for a reversible system [31] the modified electrode surface area for CoTOBPc–SWCNT–GCE was found to be 0.18 cm^2:

$$I_p = 2.69 \times 10^5 n^{3/2} A_{sg} D^{1/2} C \upsilon^{1/2} \quad (1)$$

where n is the number of electrons transferred ($n = 1$), D is the diffusion coefficient of $[Fe(CN)_6]^{3-}$ (7.6×10^{-6} cm^2/s) [31]), υ is the scan rate, A is the modified electrode surface area, C is the bulk concentration of $[Fe(CN)_6]^{3-}$ (1×10^{-3} mol L^{-1}).

3.3.2. Electrode behaviours in pH 4 buffer solution and surface coverage

Fig. 2 shows the cyclic voltammograms for bare GCE, SWCNT–GCE, CoTOBPc/SWCNT–GCE, CoTOBPc and CoTOBPc–SWCNT–GCE, all in pH 4 buffer. The oxidation of amitrole was found to be optimum at this pH, hence it was employed in these studies [19]. CoTOBPc–SWCNT–GCE, CoTOBPc/SWCNT–GCE, CoTOBPc–GCE) show broad peaks between 0.6 and 0.9 V which are associated with Co^{III}/Co^{II} process in comparison with literature [32]. Increases in peak currents and shifts in peak potentials towards more positive values were observed for the conjugate as the scan rates increased. A linear relationship of the plot of background corrected current versus sweep rate (100–800 mV/s) for CoTOBPc–SWCNT–GCE was observed, inset Fig. 2. This behaviour is

Table 1
Summary of spectroscopic data, voltammetric and EIS parameters.

Electrode	$\lambda_{Q\ band}$ (nm) DMF	ΔE (mV) $[Fe(CN)_6]^{3-/4-}$	E_p (V) Amitrole	R_{CT} (kΩ)	n	k_{ET} (cm s^{-1})
Bare GCE		64	0.92	49.40	0.62	5.39×10^{-8}
CoTOBPc	650 nm	80	0.90	30.43	0.61	8.75×10^{-8}
SWCNT		69	0.86	27.96	0.62	9.52×10^{-8}
CoTOBPc/SWCNT	667 nm	75	0.84	25.13	0.68	1.06×10^{-5}
CoTOBPc–SWCNT	670 nm	61	0.81	17.72	0.66	1.50×10^{-5}

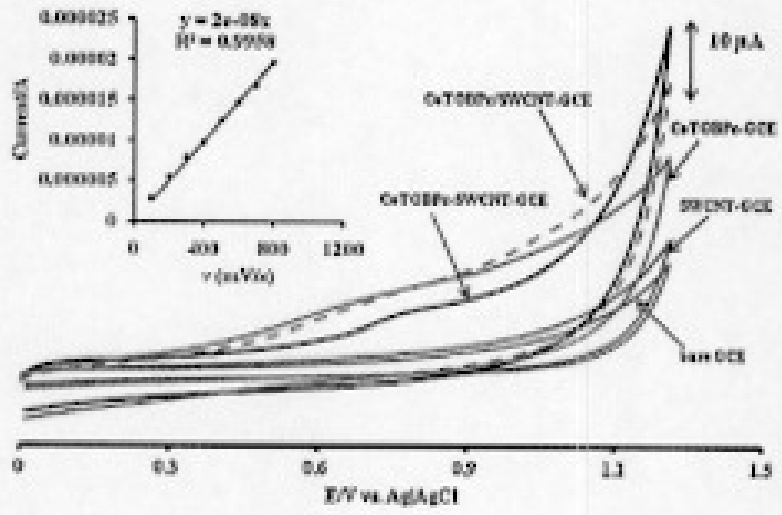

Fig. 2. Cyclic voltammograms in pH 4 buffer for bare GCE, SWCNT–GCE, CoTOBPc/SWCNT–GCE, CoTOBPc–GCE and CoTOBPc–SWCNT–GCE. Inset: plot of current versus scan rate for CoTOBPc–SWCNT. Scan rate = 100 mV/s.

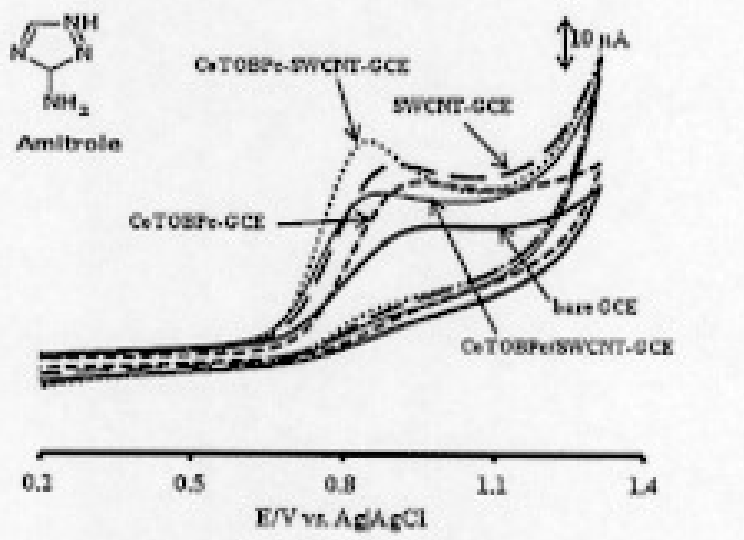

Fig. 3. Cyclic voltammograms in 1 mM amitrole (in pH 4 buffer) for bare GCE, CoTOBPc/SWCNT–GCE, CoTOBPc–GCE, SWCNT–GCE and CoTOBPc–SWCNT–GCE. Scan rate = 100 mV/s.

typical of surface-immobilized species. From the slope of this linear plot and using Eq. (2) [33], the surface coverage was calculated.

$$I_p = \frac{n^2F^2}{4RT}\upsilon A_{eff}\Gamma_{MPc} \quad (2)$$

where I_p is the background corrected peak current, n is the number of transferred electrons, F is the Faraday constant, Γ_{MPc} is the film surface coverage, A is the modified electrode surface area (0.18 cm^2 from above), υ is the scan rate, R is the gas constant and T is the temperature. The value of the surface coverage was found to be 1.20×10^{-10} mol cm^{-2} and this is slightly higher than a monolayer surface coverage [34] for Pc molecule lying flat on the electrode surface. The higher surface area could be due to the presence of the SWCNT.

3.4. Detection of amitrole

3.4.1. Comparative cyclic voltammetric responses towards amitrole

The bare GCE, CoTOBPc–SWCNT–GCE, CoTOBPc/SWCNT–GCE, SWCNT–GCE and CoTOBPc–GCE were used in the oxidation of amitrole (inset in Fig. 3) for comparative purposes, Fig. 3. Since the complex, CoTOBPc–SWCNT is a combination of CoTOBPc and SWCNTs it was reasonable to assess their individual oxidation potentials to enable conclusive deductions to be made about their catalytic efficiencies relative to CoTOBPc–SWCNT electrode. The observed peaks in the region 0.8–1.0 V are due to the oxidation of amitrole as observed in other studies [18]. The oxidation peaks (Table 1) for amitrole were observed at 0.92 V, 0.81 V, 0.84 V, 0.86 V and 0.90 V (versus Ag|AgCl) for the bare GCE, CoTOBPc–SWCNT–GCE, CoTOBPc/SWCNT–GCE, SWCNT–GCE and CoTOBPc–GCE, respectively. Compared to the oxidation of amitrole on FeTAPc-SWCNT (TAPc = tetraaminophthalocyanine) conjugates [8] that contain amide linkages which occurred around 0.90 V (versus Ag|AgCl) there is a huge improvement in the catalysis of the same compound on CoTOBPc–SWCNT–GCE (0.81 V), which contains imide bonds. The CoTOBPc–SWCNT–GCE (Fig. 3), shows higher oxidation currents at reduced oxidation overpotentials compared to the rest of the electrodes, confirming its better catalytic properties. The sharp rise in current at the inception of the oxidation of amitrole is a clear indication of the good electrocatalytic properties of CoTOBPc–SWCNT electrode. Due to the nature of chemical linking, conjugates form three-dimensional surface arrays on the electrode surface. These arrays have very large surface areas and are highly porous, therefore easily accessed by the analyte, resulting in the easy oxidation of amitrole on CoTOBPc–SWCNT–GCE. As shown from Fig. 3, the oxidation of amitrole occurs on the CoTOBPc–SWCNT–GCE at potentials for the $Co^{III}Pc$ process, hence it is catalysed by these species. From Fig. 3 it can be confirmed that the CoTOBPc–SWCNT electrode is superior relative to the other electrodes hence it was further used in the oxidation kinetic studies of amitrole.

Fig. 4 (Supporting information) shows the variations in stability of the following electrodes CoTOBPc (a), CoTOBPc/SWCNT (b), CoTOBPc–SWCNT (c), SWCNT (d), and bare GC (e) in the presence of 1 mM amitrole (pH 4) over 20 continuous cycles. The order in the drop in current from cycle 1 to 2 is as follows: SWCNT–GCE (13. 8 μA) > CoTOBPc–SWCNT–GCE (13.4 μA) > bare GCE (11.8 μA) > CoTOBPc/SWCNT–GCE (9.0 μA) > CoTOBPc–GCE (8.7 μA). The fouling of the electrode is a continuous process. Successful regeneration of CoTOBPc–SWCNT–GCE (Fig. 4 inset, Supporting information) was achieved by shaking the electrode in methanol and scanning (using cyclic voltammetry) in pH 4 buffer solution. Methanol dissolves away all the amitrole oxidation products. The regeneration and reproducibility of the voltammograms confirmed little or no leaching of the catalyst. This minimal leaching is attributed to the dual combination of strong π–π interactions between the GCE and the CoTOBPc and SWCNT components of the conjugate. Under conditions of continual use and storage in pH 4 buffer, the electrode has a life span of more than three months. Similarly other electrodes could be regenerated though the life spans were less than that for CoTOBPc–SWCNT–GCE.

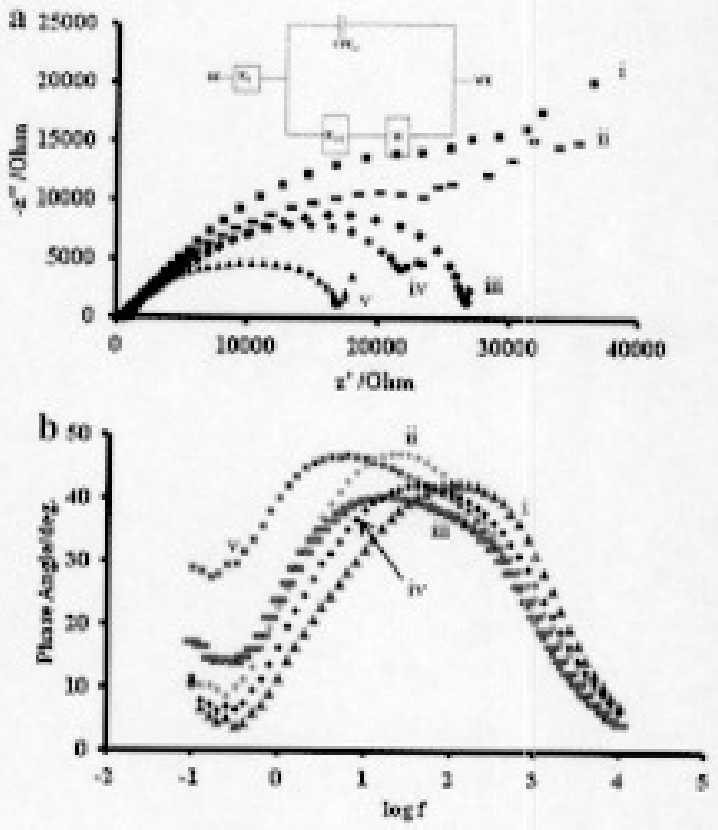

Fig. 4. (a) Nyquist plot of (i) bare GCE, (ii) CoTOBPc–GCE, (iii) SWCNT–GCE, (iv) CoTOBPc/SWCNT–GCE and (v) CoTOBPc–SWCNT–GCE recorded in 1.0 mM amitrole (pH 4 buffer). Inset for (a) suggested Randle equivalent circuit model for the impedance spectrum (RE = reference electrode, WE = working electrode) and (b) typical Bode plots (phase angle versus log *f*) obtained for (i) bare GCE, (ii) CoTOBPc/SWCNT–GCE, (iii) SWCNT–GCE, (iv) CoTOBPc and (v) CoTOBPc–SWCNT in 1 mM amitrole (pH 4 buffer).

3.4.2. Kinetic studies of amitrole on CoTOBPc–SWCNT–GCE

Fig. 5a (Supporting information) shows the evolved amitrole voltammograms on CoTOBPc–SWCNT–GCE as the scan rate increased (from 50 mV/s to 1000 mV/s). The amitrole oxidation peak shifted towards the positive potential, an indication of irreversibility of the reaction. A linear plot of current versus root of scan rate (Fig. 5a, inset, Supporting information) confirmed that the irreversible catalytic oxidation of amitrole is diffusion controlled.

The relationship between peak potential and scan rate for an irreversible diffusion-controlled process is given by Eq. (3) [35]:

$$E_p = \frac{2.3RT}{2(1-\alpha)n_\alpha F}\log \upsilon + K \quad (3)$$

where α is the transfer coefficient, n_α is the number of electrons involved in the rate determining step, υ is the scan rate, K is a constant and the remaining symbols have their usual meaning. Plot of E_p versus $\log \upsilon$ (Fig. 5b, Supporting information) gave a linear relationship represented by Eq. (4) with a Tafel slope of 200 mV decade^{-1}.

$$E_p = 0.1006(\text{V/decade})\log \upsilon + 0.6752V \quad (4)$$

High Tafel slopes have no kinetic meaning and are consistent with substrate-catalyst interactions in a reaction intermediate [20] or simply passivation of the electrode surface. Tafel slopes much greater than the normal 30–120 mV decade^{-1} for one electron rate determining steps are known [36] and have been also been linked to chemical reactions coupled to electrochemical steps [36].

3.4.3. Electrochemical impedance spectroscopy

A three electrode electrochemical impedance spectroscopy (EIS) was used to probe the redox and structural features of the different working electrodes (WE). Fig. 4a shows the Nyquist plots obtained in 1 mM amitrole. The bare GCE, CoTOBPc–GCE, CoTOBPc–SWCNT–GCE and SWCNT–GCE displayed identical semi-circular Nyquist plots with a straight line portion at lower frequencies. Semi-circles represent a combination of charge transfer resistance and the double layer capacitance of the electrode modifiers and represent kinetically controlled movement of electrons [37]. The straight line portion represents the Warburg impedance which takes into account the frequency dependence on diffusion transportation to the electrode surface. The representative circuit for the Nyquist plots (Fig. 4a) is shown in Fig. 4a (inset), where R_S, CPE_{dl}, R_{CT} and W represent solution resistance, a constant phase element (corresponding to the double layer capacitance at the electrode surface), the charge transfer resistance and the Warburg impedance, respectively.

The diameter of the semi-circle is proportional to the charge transfer resistance, hence electron transfer properties can be determined. The order of decrease of electron transfer efficiencies (in the form of decrease in R_{CT}) is as follows: CoTOBPc–SWCNT–GCE > CoTOBPc/SWCNT–GCE > SWCNT–GCE > CoTOBPc–GCE > bare GCE (Fig. 4a). Such a trend was also observed from the cyclic voltammetry of amitrole on different electrodes (Table 1), where CoTOBPc–SWCNT–GCE showed reduced potentials and improved currents.

At the frequency region of the impedance under study, the charge-transfer resistance (R_{CT}) decreased (Table 1) for the electrode modifiers due to facilitation of the electron-transfer, an indication that films form high electron conduction pathways between the electrode and electrolyte/analyte as observed elsewhere [38]. Table 1 summarizes the various parameters obtained for the different electrodes that were used for the oxidation of amitrole.

The *n*-values are greater than 0.6 but <1, an indication of the non-capacitative nature of the electrodes. The apparent electron-transfer rate constants, k_{app}, were obtained using Eq. (5) [39].

$$k_{app} = \frac{RT}{F^2 R_{CT} C} \quad (5)$$

where C is the concentration of amitrole (1×10^{-6} mol cm^{-3}), with R, T and F having their usual meanings. As reflected in its k_{app} and R_{CT} values, the CoTOBPc–SWCNT–GCE has the fastest electron transfer properties towards amitrole compared to other electrodes investigated in this work. However, it is interesting to note that SWCNT on their own show a relatively higher electron transfer rate constant compared to the CoTOBPc and bare GCE. Therefore it is not surprising that a combination of the CoTOBPc and SWCNTs (as a mixture or chemically linked) results in higher apparent rate constants, Table 1, confirming the already predicted synergism between the two compounds.

The Bode plot (plot of phase-shift (θ) versus the log *frequency*), Fig. 4b, was used to obtain frequency related information, which cannot be obtained from the Nyquist plot. These Bode plots confirmed the structural differences of the various electrodes. All the electrodes showed Bode angles of less than 50°, an indication of their non-capacitative nature, hence permeable to ions [40]. Changes in the phase angles and frequencies relative to the bare GCE observed on all the electrodes confirmed that the oxidation of amitrole was taking place at modified surfaces rather than on the bare GCE surface.

3.4.4. Chronoamperometric studies

Catalytic rate constants are measures of how fast redox processes proceed at the electrode/analyte interface. The rate of oxidation of amitrole was evaluated on the CoTOBPc–SWCNT–GCE through chronoamperometric studies. Fig. 5 shows chronoamperograms for (i) blank, pH 4 buffer only, (ii) 5 μM, (iii) 10 μM, (iv) 15 μM, (v) 20 μM and (vi) 25 μM of amitrole (ii–vi in pH 4 buffer) produced on polarized CoTOBPc–SWCNT–GCE. Fig. 5, inset, a plot

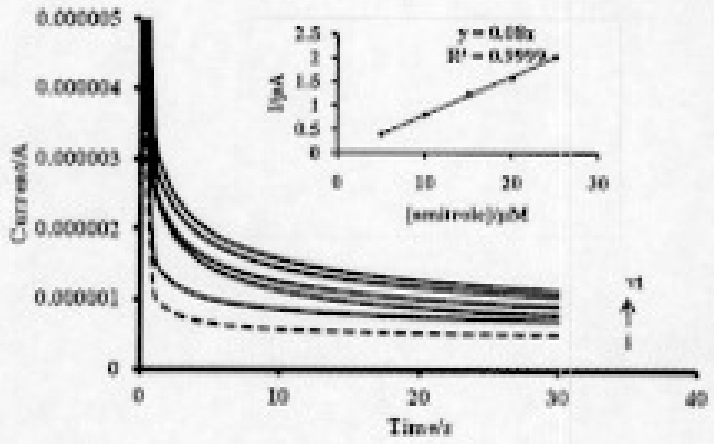

Fig. 5. Chronoamperograms obtained at a polarized CoTOBPc–SWCNT–GCE in (i) pH 4 buffer and in amitrole (pH 4): (ii) 5 μM, (iii) 10 μM, (iv) 15 μM, (v) 20 μM and (vi) 25 μM. Inset plot of current versus amitrole concentration.

of current versus the concentration of amitrole shows a linear relationship with a sensitivity of 1.13 A mol^{-1} L cm^{-2}, an indication that this electrode can be successfully employed in the analysis of amitrole.

At intermediate times (t = 1–5 s) used in this study, the catalytic current (I_{cat}) is dominated by the rate of the electro-catalysed oxidation of amitrole on the redox reaction sites of the surface confined CoTOBPc–SWCNT species. The catalytic rate constant can be determined according to a literature method, Eq. (6) [35]:

$$\frac{I_{cat}}{I_{buf}} = \gamma^{1/2}\pi^{1/2} = \pi^{1/2}(kC)^{1/2} \quad (6)$$

where I_{cat} and I_{buf} are currents in the presence and absence of amitrole, k is the catalytic rate constant (M^{-1} s^{-1}), C is the bulk concentration of amitrole and t the elapsed time in seconds. Fig. 6a (Supporting information) shows the linear plots of I_{cat}/I_{buf} versus $t^{1/2}$ for amitrole. From the slopes of plots in Fig. 6a (Supporting information), plots of the square of slopes versus concentration were obtained (Fig. 6b, Supporting information) whose slopes are equal to πk. The linear equation is shown by Eq. (7).

$$y = 0.005[Amitrole]\left(\frac{s^{-1}}{\mu M}\right) + 0.237\,s^{-1}, \quad R^2 = 0.9952 \quad (7)$$

The value of k was found to be 1.6×10^3 M^{-1} s^{-1}, a value higher than (but with the same order of magnitude) 1.2×10^3 M^{-1} s^{-1} obtained on CoTCPc-SWCNT(linked)–GCE [41] (TCPc = tetracarboxyphthalocyanine), showing that the oxidation of amitrole is faster on CoTOBPc–SWCNT–GCE. A plot of $\log I_p$ versus log[concentration] (figure not shown) indicated that electrocatalysis of amitrole is first order. This implies that one analyte molecule interacts with one molecule of CoTOBPc–SWCNT. Using the already stated arguments and also that Co(III)/Co(II) process is implicated in the catalysis, the proposed mechanism for the catalytic oxidation of amitrole is by Eqs. (8) and (9):

$$Co(II)TOBPc^{-2}\text{–}SWCNT \xrightarrow{-e^-} [Co(III)TOBPc^{-2}]^{+1}\text{–}SWCNT \quad (8)$$

$$2[Co(III)TOBPc^{-2}]^{+1}\text{–}SWCNT + Amitrole \rightleftharpoons 2Co(II)TOBPc^{-2}\text{–}SWCNT + \text{amitrole oxidation products} \quad (9)$$

The oxidation of amitrole occurs in the stability range of the $Co(III)TOBPc^{-2}$ species, hence the latter is involved in the mediation process. Eq. (9) shows the oxidation of amitrole and regeneration of the CoTOBPc–SWCNT electrocatalyst. The oxidation of amitrole is a known two electron process [20]. The SWCNT is there to increase the rate of electron transfer at the electrode surface.

4. Conclusions

CoTOBPc–SWCNT conjugates were successfully synthesized, characterized and applied for the study of the electrochemical behaviour of amitrole. Various kinetic parameters such as the apparent rate constant and kinetic rate constant for amitrole were determined using electrochemical impedance spectroscopy and chronoamperometric studies, respectively. Chemically linking CoTOBPc to SWCNTs produced very good platforms for the easy electrocatalytic oxidation of amitrole. This electrode showed relatively good resistance to passivation from amitrole and its oxidation products and is easily regenerated through shaking in methanol and cyclisation in pH 4 buffer.

Acknowledgements

This work was supported by the Department of Science and Technology (DST) and National Research Foundation (NRF), South Africa through DST/NRF South African Research Chairs Initiative for Professor of Medicinal Chemistry and Nanotechnology as well as Rhodes University. TM would like to thank Rhodes University for the post-doctoral fellowship and Midlands State University (Zimbabwe) for the Leave of Absence. YA thanks to Istanbul Technical University, DPT and TUBITAK.

Appendix A. Supplementary data

Supplementary data associated with this article can be found, in the online version, at doi:10.1016/j.electacta.2012.02.041.

References

[1] H. Dai, Acc. Chem. Res. 35 (2002) 1035.
[2] R.H. Baughman, A. Zakhidov, W.A. De Heer, Science 297 (2002) 787.
[3] P.M. Ajayan, Chem. Rev. 99 (1999) 1787.
[4] Y. Lin, F. Lu, J. Wang, Electroanalysis 16 (2004) 145.
[5] G. Rivas, M.D. Rubianes, M.C. Rodriguez, N.F. Ferreyra, G.L. Luque, M.L. Pedano, S.A. Miscoria, C. Parrado, Talanta 74 (2007) 291.
[6] A.C. Ontiko, P.M. Armistead, S.R. Kircus, H.H. Thorp, Inorg. Chem. 38 (1999) 1842.
[7] J. Wang, J.R. Fernandes, L.T. Kubota, Anal. Chem. 70 (1998) 3699.
[8] T. Mugadza, T. Nyokong, Electrochim. Acta 55 (2010) 2606.
[9] T. Mugadza, T. Nyokong, Electrochim. Acta 54 (2009) 6347.
[10] D.A. Geraldo, C.A. Togo, J. Limson, T. Nyokong, Electrochim. Acta 53 (2008) 8051.
[11] A.S. Adekunle, J. Pillay, K.I. Ozoemena, Electrochim. Acta 55 (2010) 4319.
[12] J. Pillay, K.I. Ozoemena, Electrochim. Acta 52 (2007) 3630.
[13] Y. Yuan, B. Zhao, Y. Jeon, S. Zhong, S. Zhou, S. Kim, Bioresour. Technol. 102 (2011) 5849.
[14] P. Mashazi, T. Mugadza, N. Sosibo, P. Mdlulia, S. Vilakazi, T. Nyokong, Talanta 85 (2011) 2202.
[15] J.F. Silva, S. Griveau, C. Richard, J.H. Zagal, F. Bedioui, Electrochem. Commun. 9 (2007) 1629.
[16] W. Chidawanyika, T. Nyokong, Carbon 48 (2010) 2831.
[17] M. Fielding, D. Barceló, A. Helweg, S. Galassi, L. Tortenson, van Zoonen, R. Wolter, G. Angeletti, Pesticides in ground and drinking water, Water Pollution Research Report 27, Commission of the European Communities, Directorate-General for Science, Research and Development, 1991.
[18] M. Chicharro, A. Zapardiel, E. Bermejo, M. Moreno, E. Madrid, Anal. Bioanal. Chem. 373 (2002) 277.
[19] M. Siswana, K.I. Ozoemena, T. Nyokong, Talanta 69 (2006) 1136.
[20] J.-M. Zen, A. Senthil Kumar, M.-R. Chang, Electrochim. Acta 45 (2000) 1691.
[21] D. Wöhrle, M. Eskes, K. Shigehara, A. Yamada, Synthesis (1993) 194.
[22] J. Liu, A.G. Rinzler, H. Dai, J.H. Hafner, R.K. Bradley, P.J. Boul, A. Lu, T. Iverson, K. Shelimov, C.B. Huffman, F. Rodriguez-Macias, Y.-S. Shon, T.R. Lee, D.T. Colbert, R.E. Smalley, Science 280 (1998) 1253.
[23] R.C. Haddon, C. Jiang, United States Patent 6331126, 2001.
[24] X. Zhang, Y. Feng, S. Tang, W. Feng, Carbon 48 (2010) 211.
[25] Y. Wang, N. Hu, Z. Zhou, D. Xu, Z. Wang, Z. Yang, H. Wei, E.S-W. Kong, Y. Zhang, J. Mater. Chem. 21 (2011) 3779.
[26] H. Peng, L.B. Alemany, J.L. Margrave, V.N. Khabashesku, J. Am. Chem. Soc. 125 (2003) 15174.
[27] B.N. Achar, K.S. Lokesh, J. Organomet. Chem. 689 (2004) 2601.
[28] Z. Hao, Q.F. Liu, J.B. Wang, J. Compos. Mater. 44 (2010) 389.
[29] A.B.P. Lever, E.R. Milaeva, G. Speier, in: C.C. Leznoff, A.B.P. Lever (Eds.), Phthalocyanines: Properties and Applications, vol. 3, VCH Publishers, New York, 1993, p. 1.
[30] A. Erdogmus, I.A. Akinbulu, T. Nyokong, Polyhedron 29 (2010) 2352.

[31] J.J. Gooding, V.G. Praig, E.A.H. Hall, Anal. Chem. 70 (1998) 2396.
[32] M.P. Siswana, K.I. Ozoemena, T. Nyokong, Electrochim. Acta 52 (2006) 114.
[33] D. Martel, N. Sojic, A. Kuhn, J. Chem. Educ. 79 (2002) 349.
[34] S. Griveau, V. Albin, T. Pauporté, J.H. Zagal, F. Bedioui, J. Mater. Chem. 12 (2002) 225.
[35] A.J. Bard, L.R. Faulkner, Electrochemical Methods, John Wiley and Sons, New York, 2001.
[36] C.A. Caro, F. Bedioui, J.H. Zagal, Electrochim. Acta 47 (2002) 1489.
[37] S. Majdi, A. Jabbari, H. Heli, A.A. Moosavi-Movahedi, Electrochim. Acta 52 (2007) 4622.
[38] Y. Liu, M. Wang, F. Zhao, Z. Gun, H. Chen, S. Dong, J. Electroanal. Chem. 581 (2005) 1.
[39] E. Sabatani, I. Rubinstein, J. Phys. Chem. 91 (1987) 6663.
[40] V. Lakshminarayanan, U.K. Sur, Pramana 61 (2003) 361.
[41] T. Mugadza, T. Nyokong, Synth. Met. 160 (2010) 2089.